ENGINEERING

Ion sensing with single charge resolution using sub–10-nm electrical double layer–gated silicon nanowire transistors

Qitao Hu[1], Si Chen[1], Paul Solomon[2]*, Zhen Zhang[1]*

Electrical sensors have been widely explored for the analysis of chemical/biological species. Ion detection with single charge resolution is the ultimate sensitivity goal of such sensors, which is yet to be experimentally demonstrated. Here, the events of capturing and emitting a single hydrogen ion (H^+) at the solid/liquid interface are directly detected using sub–10-nm electrical double layer–gated silicon nanowire field-effect transistors (SiNWFETs). The SiNWFETs are fabricated using a complementary metal-oxide-semiconductor compatible process, with a surface reassembling step to minimize the device noise. An individually activated surface Si dangling bond (DB) acts as the single H^+ receptor. Discrete current signals, generated by the single H^+-DB interactions via local Coulomb scattering, are directly detected by the SiNWFETs. The single H^+-DB interaction kinetics is systematically investigated. Our SiNWFETs demonstrate unprecedented capability for electrical sensing applications, especially for investigating the physics of solid/liquid interfacial interactions at the single charge level.

INTRODUCTION

Electrical sensors for chemical/biological substances have attracted great interest owing to their capability of label-free, real-time, and rapid analysis, as well as the possibility of miniaturization (*1*). Ion detection with single charge resolution is a highly sought-after goal for the electrical sensors. It can provide a powerful technology to resolve individual quanta of analyte and to investigate the physics of solid/liquid interfacial interactions at the single charge level. The nanoscale field-effect transistor (FET) is a promising candidate for such goal because of its superior charge sensitivity (*2*–*6*). Electrical detections of a single DNA (*7*, *8*) or protein (*9*) molecule in liquid samples have been reported using FET sensors based on the bottom-up fabricated self-assembled nanostructures, such as nanowires (*9*) or carbon nanotubes (*7*, *8*). However, direct detection of a single charge in the liquid has not been reached in the reports. In addition, the complexity of the device fabrication based on self-assembled nanostructures greatly limits the large-scale integration and applications (*10*, *11*).

In contrast to the bottom-up approach, top-down fabricated silicon nanowire (SiNW) FETs are fully compatible with the standard complementary metal-oxide-semiconductor (CMOS) fabrication technology. These SiNWFET sensors have been used for detection of ions (*12*–*14*) and molecules (*15*, *16*) with ultrahigh sensitivity. The potential for single charge detection using such SiNWFET sensors was also theoretically predicted many years ago (*17*). However, because of the limitation in signal-to-noise ratio (SNR), electrical ion detection at the single charge level remains to be experimentally demonstrated. A SiNWFET sensor is normally gated via an oxide-based gate dielectric layer, which inevitably separates the impinging target charge from the channel and thus suppresses the signal generation. On the other hand, the top-down process induced roughness and defects on the SiNW surface contribute considerably to the intrinsic device noise (*18*). In addition to the challenges of SNR, to time-resolve a single target-receptor interaction event on a sensor surface, it is also very critical to limit the total number of receptors to a few.

Here, we designed and fabricated sub–10-nm SiNWFETs with the standard top-down Si fabrication method. A H_2 annealing process was used to reassemble an atomically smooth SiNW surface and thus minimize the defect-induced intrinsic device noise. Our SiNWFET sensors were made with a gate oxide–free configuration, in which the electrical double layer (EDL) in the liquid acted as the gate insulator. This configuration, with a clean silicon sensing surface and no intervening oxide, enabled the target charge binding directly on the channel surface and therefore improved the detection sensitivity. In addition, most of the Si dangling bonds (DBs) on the SiNW surface were passivated by covalent H-terminations during the native oxide etching step in buffered hydrogen fluoride (BHF). The few remaining DBs could be individually activated as single hydrogen ion (H^+) receptors via gate voltage modulation. The single H^+-DB interactions were directly detected by our EDL-gated SiNWFETs, represented as discrete drain-to-source current (I_{DS}) switching between two levels. The kinetics of the interactions and its correlation with the energy barrier at the solid/liquid interface were systematically investigated. The signal transduction mechanism was also identified. Our EDL-gated SiNWFET sensors demonstrate the unprecedented capability to investigate the physics of solid/liquid interface at the single charge level and hold great potential for future biochemical sensing applications.

RESULTS

Process optimization for sub–10-nm SiNWFETs

A three-dimensional schematic of the sub–10-nm gate oxide–free SiNWFET is shown in Fig. 1A. The SiNWFET was fabricated on a (100) silicon-on-insulator (SOI) wafer with the standard Si process technology. The source (S) and drain (D) regions of the SiNWFET are heavily *n*-doped (yellow), while the SiNW channel consists of a

[1]Division of Solid State Electronics, Department of Electrical Engineering, Uppsala University, BOX 65, SE-75103 Uppsala, Sweden. [2]IBM Thomas J. Watson Research Center, Yorktown Heights, NY 10598, USA.
*Corresponding author. Email: zhen.zhang@angstrom.uu.se (Z.Z.); solomonp@us.ibm.com (P.S.)

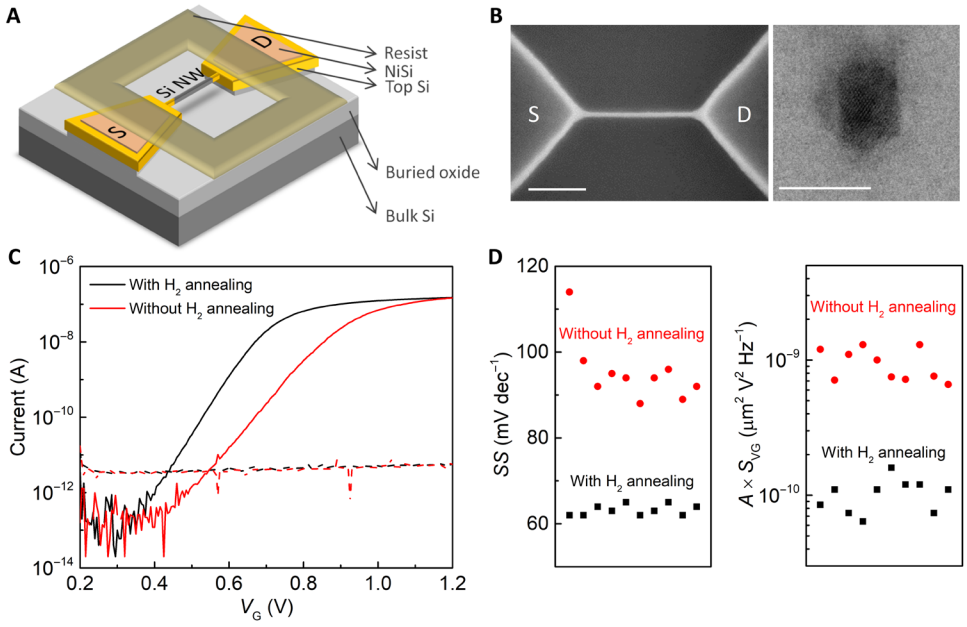

Fig. 1. SiNWFET fabrication process optimization. (**A**) Three-dimensional schematic of a SiNWFET. The SiNW consists of a lightly *p*-doped region (gray) in the center and a heavily *n*-type region (yellow) on each side. (**B**) SEM image (left; scale bar, 100 nm) and cross-sectional TEM image (right; scale bar, 10 nm) of a SiNWFET with H_2 annealing. (**C**) Typical transfer characteristics of SiNWFETs with and without H_2 annealing measured in 1 mM KCl at V_{DS} = 10 mV. The solid and dashed lines mean I_{DS} and gate leakage current, respectively. (**D**) Summary of SS (left) and $A \times S_{VG}$ at 10 Hz (right) of 10 SiNWFETs with and without H_2 annealing measured in 1 mM KCl at V_{DS} = 10 mV.

150-nm-long lightly doped *p*-type region (gray). Detailed description of the fabrication process can be found in Materials and Methods and figs. S1 and S2.

To detect the single H^+ capture/emission events, the intrinsic device noise of SiNWFET must be lower than the single charge signal. The intrinsic noise of SiNWFET strongly depends on the defect density on SiNW surface and is inversely proportional to gate area (section S3) (*18*–*20*). For our sub–10-nm SiNW, the process-induced surface roughness becomes comparable with SiNW diameter as shown by the scanning electron microscope (SEM) image in fig. S3A. Such roughness and its associated surface defects could contribute notably to the device noise. The surface roughness problem was addressed by annealing the SiNW structure in a H_2 ambient. The annealing facilitates migration of surface Si atoms to the lower-energy sites and a reassembly of the surface at the temperature well below the Si melting point (*21*, *22*). Such reassembly process removes the process-induced surface defects and leads to atomically smooth channel surface, as evidenced by the SEM image of the SiNWFET after H_2 annealing in Fig. 1B (left). In addition, the SiNW channel diameter is further reduced because of the migration of Si atoms on the SiNW surface to the large-size S/D pads to lower the total free energy (fig. S3B) (*21*). A cross-sectional transmission electron microscope (TEM) image of the smoothed SiNW channel is shown in Fig. 1B (right). The channel width and height measured from the image are 7 and 9 nm, respectively.

After fabrication, the SiNWFETs were measured in an electrolyte containing 1 mM KCl. A gate voltage (V_G) was applied via an Ag/AgCl reference electrode, with the EDL at the SiNW/electrolyte interface acting as the gate dielectric layer. Figure 1C depicts the I_{DS} versus V_G curves of the SiNWFETs with and without H_2 annealing. Extracted subthreshold slopes (SS) of 10 devices on the same chip are plotted in Fig. 1D (left). H_2 annealing indeed greatly improved the electrical performance of the SiNWFETs, as evidenced by their near-ideal SS ~60 mV dec^{-1} and much-reduced spread in threshold voltage (V_T) among the devices (fig. S4). The gate-referred voltage noise S_{VG} at 10 Hz, after gate area (A) normalization, was lowered by about one order of magnitude by H_2 annealing, i.e., on average, from ~1×10^{-9} to ~1×10^{-10} $\mu m^2\ V^2\ Hz^{-1}$ (Fig. 1D, right). Note that $A \times S_{VG}$ achieved in this work is comparable to or even lower than some of the state-of-the-art SiNWFETs (*15*, *23*). Output characteristics of the SiNWFETs and more noise data can be found in figs. S5 and S6, respectively.

The number of H^+ receptors, i.e., surface Si DBs, on the SiNW channel is critical for single charge detection and therefore is carefully engineered in this work. The Si atom has four valence electrons and requires four bonds to saturate the valence shell. On the SiNW surface, nonsaturated valence electrons could form DBs, which can capture H^+ from the electrolyte. The density of these DBs on (100) Si surface is approximately 10^{14} cm^{-2} eV^{-1}. Considering the dimensions of our SiNW channel, the total number of DBs will be ~3000, which is too high for detecting single H^+. It is known that oxygen atoms can terminate the Si DBs by forming an oxide layer and lower their density to ~10^{12} cm^{-2} eV^{-1} (*24*). Upon BHF etching of the formed oxide, most of Si DBs will be passivated with covalent H-terminations, and the DB density will be further reduced to ~10^{10} cm^{-2} eV^{-1} (*25*, *26*). In our process flow, the surface DB density of the SiNW was controlled by a native oxide etching step in BHF. After being passivated in BHF, the number of DBs is estimated to be 0.3 per SiNW, suggesting a high probability of a single H^+ receptor activated on the tiny SiNW channel surface.

Detection of single H^+

Detection of single H^+ capture/emission events was conducted in a 10 mM HCl solution, with a constant gate overdrive, i.e.,

$V_G - V_T = 129.4$ mV. I_{DS} of the SiNWFET was monitored in real time, with a sampling frequency of 3 kHz. Figure 2A (top) depicts a typical I_{DS} time trace, which switches between two levels ($\Delta I_{DS} = 3$ nA). For a nanoscale transistor with gate oxide, capture and emission of a carrier by a trap at Si/oxide interface could also result in the similar I_{DS} switching (*27*, *28*). To verify whether the two-level I_{DS} switching correlates to the carrier trapping/detrapping in the solid-state FET channel, a control experiment was performed on the same SiNWFET but in deionized (DI) water. I_{DS} in the control experiment was intentionally kept the same as that in 10 mM HCl to ensure that the SiNW channel was biased to the same condition for both cases. As seen in Fig. 2A (middle), the I_{DS} trace measured in DI water does not switch between the two levels. This result excludes the possibility that the two-level I_{DS} switching is generated inside in the SiNWFET device. Another control experiment was conducted in a 10 mM KCl solution to examine the contribution of Cl^- to the I_{DS} switching. As shown in Fig. 2A (bottom), such I_{DS} switching is neither observed. This further confirms that the I_{DS} switching is generated by the interactions between H^+ (not Cl^-) and the DB. Please note that a H^+ ion binds with a water molecule and forms a hydronium ion in the liquid sample. The terms of H^+ are used for simplicity.

Our SiNWFET was biased to strong inversion with an electron conduction channel during the sensing experiments. The DB on the SiNW channel surface under strong inversion could be an electron acceptor (*29*) and saturated by an additional electron from the channel. Since the saturated DB is negatively charged, it could induce local Coulomb scattering in the SiNW channel. However, this negatively charged DB could further capture a H^+ ion from the electrolyte and become neutralized. This would weaken the local Coulomb scattering and lead to an increase of I_{DS}. Therefore, the time when I_{DS} stays at the low state is regarded as the capture time t_c, as annotated in Fig. 2A (top). Correspondingly, the emission time t_e is the time that I_{DS} remains at the high state.

Figure 2B presents a schematic of the SiNW/electrolyte interface. The SiNW surface has three different terminations, i.e., single Si DB, covalent Si-H terminations, and Si-O^- terminations on discrete native oxide islands. The EDL formed on the electrolyte side consists of a Stern layer and a diffuse layer (*30*). The capacitances of the

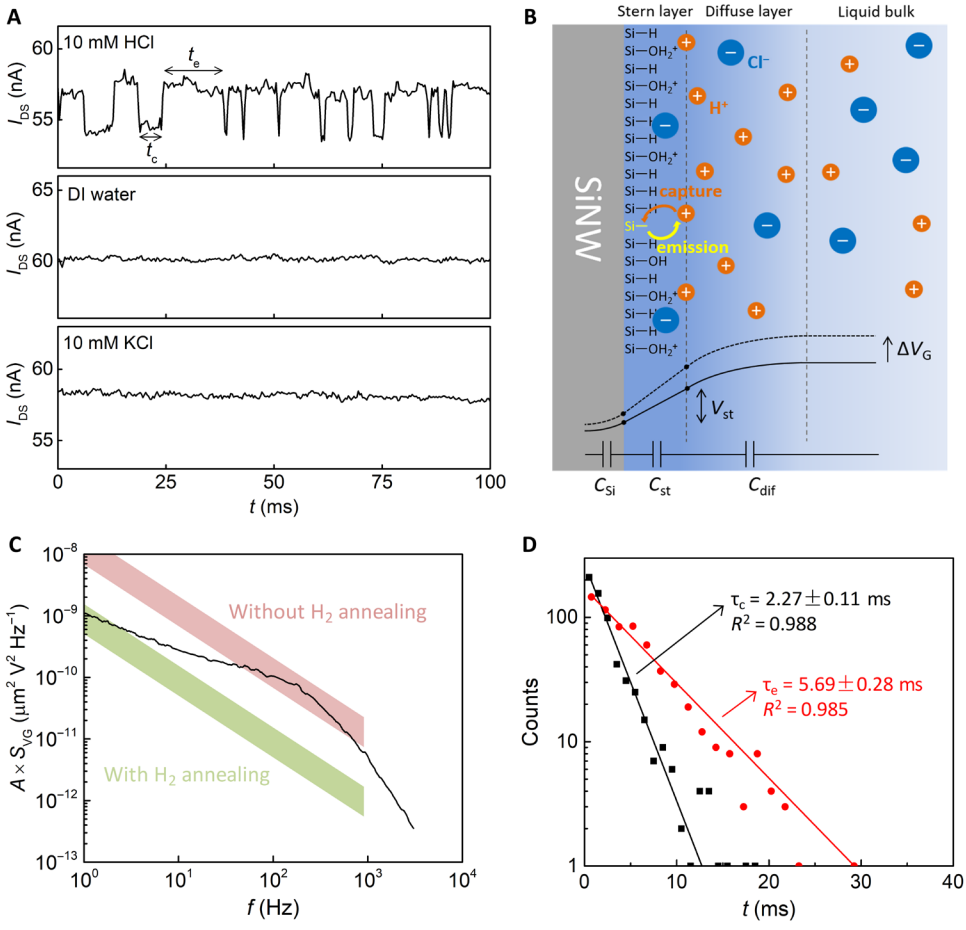

Fig. 2. Detection of single H^+-DB interactions. (**A**) I_{DS} traces recorded in 10 mM HCl, DI water, and 10 mM KCl. The sampling frequency is 3 kHz. (**B**) Schematic of SiNW/electrolyte interface. The single DB captures/emits H^+ from/to the Stern/diffuse layer interface. The total potential drop across the interface is shared by the capacitances of SiNW (C_{Si}), Stern layer (C_{st}), and diffuse layer (C_{dif}). (**C**) $A \times S_{VG}$ (black curve) generated by single H^+-DB interactions measured in 10 mM HCl, showing a Lorentzian shape with a corner frequency of ~150 Hz. The intrinsic device noise of the SiNWFET with H_2 annealing (green band) is much lower than the single charge signal, while that of the SiNWFET without H_2 annealing (red band) overwhelms the signal. (**D**) Statistical analysis of capture and emission times of single H^+-DB interaction kinetics. They are in good agreement with Poisson distribution. The time constants τ_c and τ_e are extracted from the fitted slopes. R^2, coefficient of determination.

Stern layer (C_{st}) and diffuse layer (C_{dif}) are connected in series with the SiNW capacitance (C_{Si}). The electrical potential distribution across the SiNW/electrolyte interface is also illustrated in Fig. 2B. The single DB can capture/emit a H^+ ion from/to the Stern/diffuse layer interface, which is the closest plane that H^+ can reach toward the SiNW surface. In the emission process, from the DB to the electrolyte, the single H^+ must overcome the electrical potential barrier across the Stern layer (V_{st}). The Si-O^- group on the surface can also interact with H^+ ions and generate a weak *p*H response (fig. S7), which can be well described by the site-binding and the Gouy-Chapman-Stern (GCS) models (*31*, *32*). Fitting of the *p*H response of our SiNWFET with the GCS model yields an effective –OH group density $N_{OH} = 6 \times 10^{13}$ cm^{-2}.

The time trace in Fig. 2A (top) is further analyzed in frequency domain, and its power spectrum density (PSD) is depicted in Fig. 2C, showing a Lorentzian shape profile with a corner frequency f_c ~150 Hz. In the same graph, the intrinsic device noise characteristics of SiNWFETs, with and without H_2 annealing, are also included as references. The Lorentzian hump is completely overshadowed by the intrinsic device noise of the SiNWFET without H_2 annealing, making the H^+ capture/emission events undetectable. Distributions of t_c (black rectangles) and t_e (red circles) extracted from the I_{DS} trace are presented in Fig. 2D. The distributions are in excellent agreement with Poisson statistics (*33*). Time constants of capture (τ_c) and emission (τ_e), calculated as the mean values of t_c and t_e, i.e., $\tau_c = \langle t_c \rangle$ and $\tau_e = \langle t_e \rangle$, are 2.27 and 5.69 ms, respectively.

H^+-DB interaction kinetics analysis

Figure 3A plots the I_{DS} traces of the SiNWFET (hereafter referred to as Dev. A), recorded at different $V_G - V_T$ in 10 mM HCl. Three representative I_{DS} histograms are also included, showing two discrete Gaussian peaks of each trace. A more comprehensive set of I_{DS} histograms can be found in fig. S8. Again, the peak at lower I_{DS} represents the empty state of the DB, while the one at higher I_{DS} represents the filled state. At low V_G, i.e., $V_G - V_T = 79.5$ mV, the lower peak is dominating, indicating that the DB is mostly H^+-empty. As V_G increases, the lower peak gradually diminishes, while the higher peak increases and finally becomes dominant, indicating that the DB is mostly filled with a H^+ ion. The transition from empty to filled status with increasing V_G can be quantitatively represented by the increase of occupation probability P (fig. S9A), which is calculated by the ratio of the areas of the lower and higher Gaussian peaks. As V_G increases, Stern layer shares a larger potential drop. Therefore, the energy of a H^+ ion at the DB is lowered compared to that at the

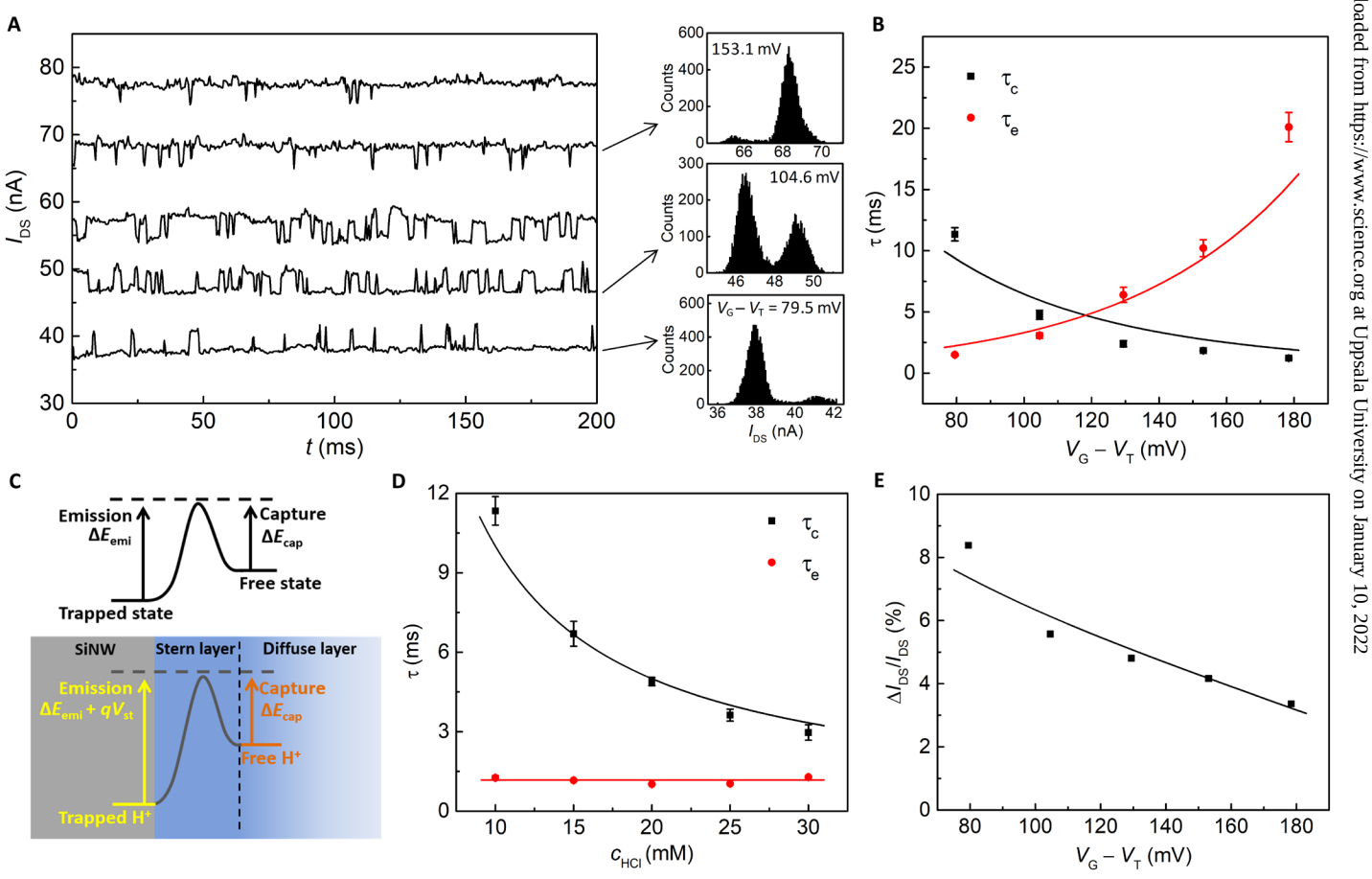

Fig. 3. Analysis of single H^+-DB interactions of Dev. A. (**A**) I_{DS} traces recorded at various $V_G - V_T$ in 10 mM HCl with 3-kHz sampling frequency. The histograms of I_{DS} present the change of occupancy status of the single DB by V_G. (**B**) Extracted τ_c and τ_e as a function of $V_G - V_T$. (**C**) Schematics of energy barriers of a general analyte-receptor reaction process (top) and the H^+ capture and emission process on the SiNWFET surface (bottom). (**D**) τ_c and τ_e as a function of HCl concentration at $I_{DS} = 40$ nA. (**E**) Relative signal amplitude as a function of $V_G - V_T$. The solid curves in (B), (D), and (E) are the fitting results.

Stern/diffuse layer interface (Fig. 2B). Consequently, the DB has a higher probability to be filled by the H^+ from the Stern/diffuse layer interface at higher V_G. PSD of the time traces in Fig. 3A is also plotted in fig. S10, all showing a Lorentzian shape profile with f_c dependent on $V_G - V_T$.

Figure 3B plots τ_c and τ_e extracted from the I_{DS} traces in Fig. 3A. τ_c decreases with increasing V_G, while τ_e shows an opposite trend. As V_G increases, the voltage drops across both diffuse layer and Stern layer are enlarged, as illustrated by the dashed line of the potential distribution in Fig. 2B. The increased potential drop in the diffuse layer will lead to an increased H^+ concentration at the Stern/diffuse layer interface (c_{Hs}), which obeys the Boltzmann distribution in the diffuse layer (*34*). Consequently, it becomes easier for the DB to capture a H^+ ion from the Stern/diffuse layer interface, leading to a shorter τ_c. At the same time, the emission of H^+ from the DB becomes more difficult because of the enlarged potential barrier across the Stern layer. Therefore, τ_e increases with increasing V_G.

The time constants can be further correlated to reaction kinetics. In a reaction between analyte and its receptor on a surface, the association (k_{on}) and dissociation (k_{off}) constants depend on the kinetic energy barriers of the capture (ΔE_{cap}) and emission (ΔE_{emi}), respectively (see Fig. 3C, top). However, for the H^+-DB interactions in our system, the potential drop across the Stern layer will add an additional barrier qV_{st} (q is the elemental charge) to the H^+ emission process, as illustrated in Fig. 3C (bottom). Therefore, τ_c and τ_e of the H^+-DB interactions can therefore be expressed as

$$\frac{1}{\tau_c} = k_{on} c_{Hs} \text{ and } \frac{1}{\tau_e} = k_{off} e^{\frac{qV_{st}}{kT}} \quad (1)$$

where k is the Boltzmann constant and T is the temperature. More details of Eq. 1 can be found in section S12. The potential and charge distribution at the SiNW/electrolyte interface (including c_{Hs} and V_{st}) can be calculated numerically using the site-binding and GCS models (see Materials and Methods) (*31*, *32*, *34*, *35*). With these inputs, the measured time constant data at different V_G can be fitted by Eq. 1, shown as solid curves in Fig. 3B. Parameters C_{st}, k_{on}, and k_{off} of Dev. A extracted from the fitting are listed in table S1.

τ_c and τ_e were also measured at different bulk HCl concentrations (c_{HCl}), ranging from 10 to 30 mM with a fixed I_{DS} of 40 nA, as shown in Fig. 3D. τ_c decreases, while τ_e does not vary with increasing c_{HCl}. This is due to the negligible *p*H sensitivity in the c_{HCl} range between 10 and 30 mM (*p*H 2 to 1.5 in fig. S7), which indicates that the change of the electrical potential across the EDL is negligible in this *p*H range. c_{Hs} then follows the increase of c_{HCl} to maintain a

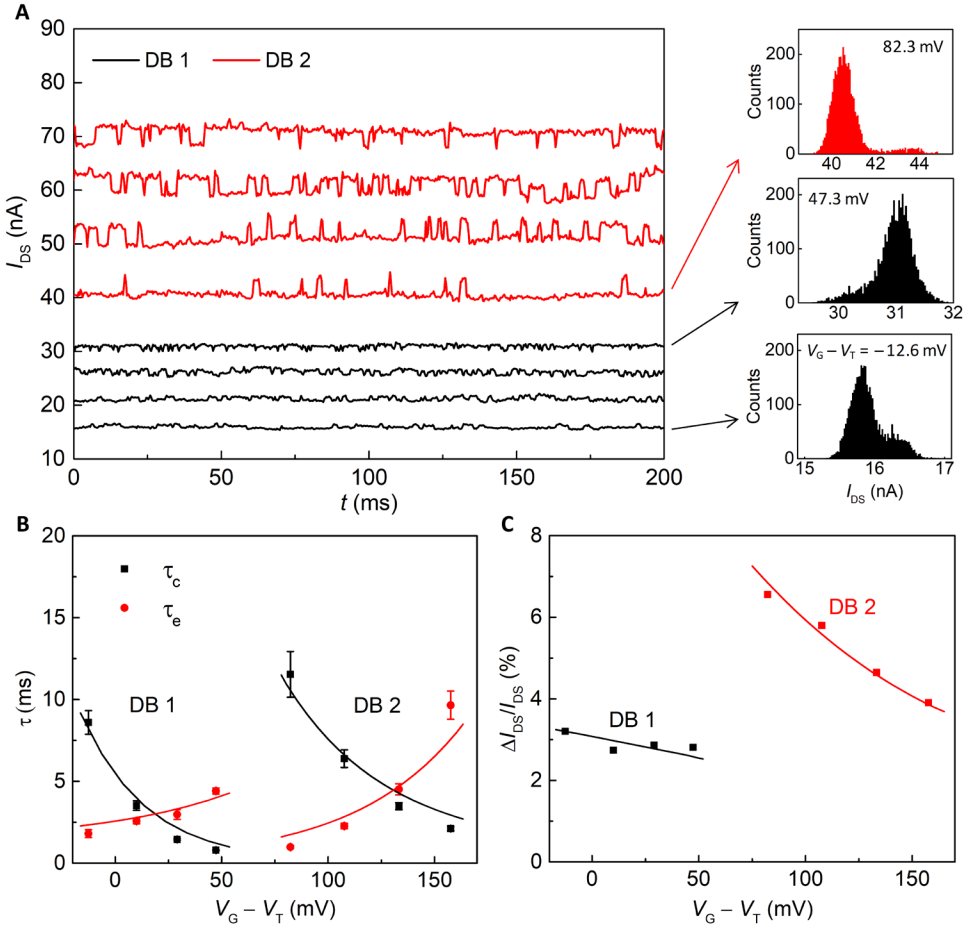

Fig. 4. One-by-one activation of DBs of Dev. B. (**A**) I_{DS} traces recorded at different $V_G - V_T$ in 10 mM HCl with 3-kHz sampling frequency. (**B**) τ_c and τ_e of the two DBs as a function of $V_G - V_T$. (**C**) Relative signal amplitude as a function of $V_G - V_T$. The solid curves in (B) and (C) are the fitting results.

constant potential drop across the diffuse layer. Higher c_{Hs} will lead to a reduced τ_c, as analytically expressed in Eq. 1. On the other hand, since V_{st} has negligible change in this *p*H range either, τ_e remains constant.

Figure 3E plots the relative amplitude ($\Delta I_{DS}/I_{DS}$) at different $V_G - V_T$, where ΔI_{DS} is the difference of the two peak values in the I_{DS} histograms. Both carrier number (ΔN) and mobility ($\Delta\mu$) fluctuations can contribute to the detected signals, i.e., $\Delta I_{DS}/I_{DS} = \Delta N/N + \Delta\mu/\mu$ (*36*). The contribution from $\Delta N/N$ induced by single H^+-DB interactions, as estimated in section S13, is negligible compared to the measured $\Delta I_{DS}/I_{DS}$. Therefore, $\Delta I_{DS}/I_{DS}$ is mainly ascribed to $\Delta\mu/\mu$ owing to the change of local Coulomb scattering strength induced by a single charge. $\Delta I_{DS}/I_{DS}$ decreases because of the reduced mobility and scattering coefficient at higher V_G (eq. S8). The measured $\Delta I_{DS}/I_{DS}$ can be well fitted by the mobility fluctuation shown as the solid curve in Fig. 3E (see section S14 for more details). The extracted scattering coefficient falls into the range of 5.4×10^{-15} to 8.4×10^{-15} V s (table S1), which is in good agreement with the reported value (~10^{-15} V s) (*37*).

One-by-one DB activation with increased V_G

The measured single H^+-DB interactions also discovered that multiple DBs on our SiNWFET surface could be activated individually. As shown in Fig. 4A, the I_{DS} traces measured on a different SiNWFET (Dev. B) can be separated into two groups depending on V_G. The first DB (DB 1) is activated at $V_G - V_T = -12.6$ mV, and its occupation status has a similar V_G dependence as Dev. A. DB 1 is mostly filled at $V_G - V_T = 47.3$ mV. As $V_G - V_T$ further increases, i.e., above 82.3 mV, the second DB (DB 2) starts to interact with H^+. Detailed histograms of the I_{DS} traces are presented in fig. S13, and their occupation probabilities are shown in fig. S9B. Figure 4B depicts τ_c and τ_e for the two DBs in Dev. B at different V_G, which can also be well fitted with the same C_{st} value in Dev. A (see the solid curves in Fig. 4B). The fitted parameters are listed in table S1. The equilibrium constant $K = k_{on}/k_{off}$ of the two DB differs by ~20 times (table S1), indicating ~78 mV energy difference between DB 1 and DB 2 in the energy bandgap. This energy difference is consistent with the difference of V_G to activate DB 1 and DB 2. As shown in Fig. 4C, $\Delta I_{DS}/I_{DS}$ of both DBs can be well fitted with mobility fluctuation, and the extracted α_{sc} is listed in table S1. α_{sc} differs largely for the two DBs, which further confirms that they are distinct DBs. Although more than one DB might exist on the SiNW surface, they can be activated individually by V_G for single charge detection.

DISCUSSION

Sub–10-nm EDL-gated SiNWFETs were fabricated using a CMOS-compatible process. The SiNW surface was smoothed with a H_2 annealing process to minimize the intrinsic device noise. The majority of the surface Si DBs were passivated with covalent H-terminations, leaving the individual DB activated on the tiny SiNW surface as the single H^+ receptor. Single H^+-DB interactions were directly detected by the SiNWFETs. On the basis of the detected single charge signals, both the kinetics of the single H^+-DB interactions and the origin of the signal amplitude were systematically investigated. This work demonstrates a silicon nanosensor with unprecedented ability to investigate the physics of the solid/liquid interface at the single charge level, which holds great potential for future biochemical sensing applications.

MATERIALS AND METHODS

Device fabrication

The sub–10-nm gate oxide–free SiNWFETs were fabricated on 100-mm SOI wafers with standard Si process technology. The SOI wafers are composed of a 55-nm-thick lightly doped *p*-type Si layer on the top of a 145-nm-thick buried oxide (BOX). The top Si layer was thinned down from 55 to 30 nm by thermal oxidation and subsequent oxide etching with HF acid. An arsenic implantation was used to form the heavily *n*-doped (n^+) source and drain terminals (S/D), while the channel region was protected by a photoresist during the implantation. The SiNWFET structure was defined by mixed lithography, i.e., the SiNW channels were pattered with a hydrogen silsesquioxane resist, while the large S/D pads were patterned with a UVN resist, followed by one-step reactive ion etching (RIE). The dopants in S/D were activated by rapid thermal processing at 1000°C for 10 s in N_2 atmosphere. To fully suspend the SiNW channel, the SOI wafers were dipped in 5% HF for 30 s to etch off 10 nm of the BOX. Afterward, thermal annealing was performed in H_2 atmosphere to enable sufficient surface Si atom reflow and therefore reparation of RIE-induced plasma damage on the SiNW channel surface. The H_2 annealing is performed in a temperature range of 800° to 880°C and a time range of 2 to 20 min. The actual annealing temperature and time depend on the SiNW channel geometry. To facilitate measurement with electrolyte, long Si (n^+) leads were designed to connect S/D of the SiNWFETs to the contact pads at the edges of the chip, on which a 10-nm-thick nickel silicide layer was formed to further reduce series resistance. A photo resist layer was used as passivation for the S/D and leads to avoid excessive leakage current in electrolyte, while the SiNW channel region was exposed for sensing in electrolyte. Last, the wafers were dipped in BHF for 5 s to remove the native oxide on the SiNW channel.

Electrical measurements

A polydimethylsiloxane container was placed on top of the Si chip for holding the solution, in which a commercial AgCl/Ag reference electrode immersed into was set at a gate potential. Transfer (I_{DS} versus V_G) and output (I_{DS} versus V_{DS}) characteristics were measured at room temperature on a probe station using a Keysight B1500A precision semiconductor parameter analyzer. The PSD and high-frequency sampling of I_{DS} were characterized using a Keysight E4727A advanced low-frequency noise analyzer. For each measurement, at a fixed I_{DS}, V_{DS} was biased at 10 mV.

Calculation of potential and charge distribution at the SiNW/electrolyte interface

Our SiNWFET has a gate-all-around structure. Under inversion, the dependence of net charge density (σ_{Si}) inside the SiNW channel on Si surface potential (ψ_{Si}) can be expressed as

$$\sigma_{Si} = -qr(n_0 e^{\frac{\psi_{Si}}{kT}} + N_A)/\gamma \quad (2)$$

Here, γ is a correction factor, i.e., $\gamma = 0.978 + 1.72 \times \exp(0.0256 \times \psi_{Si})$, dependent on the SiNW channel geometry. Its detailed derivation can be found in section S16.

H^+ concentrations at the Stern/diffuse layer interface and in the bulk solution, i.e., c_{Hs} and c_{HCl}, obey Boltzmann distribution (*34*)

$$c_{Hs} = c_{HCl} \exp\left(\frac{q(V_G - V_0 - \psi_{dif})}{kT}\right) \quad (3)$$

where ψ_{dif} is the potential at the Stern/diffuse layer boundary. To simplify the calculation, here, a constant term V_0 is introduced to sum up the potential drops across the reference electrode junction and the potential generated by the fixed charge on SiNW surface. Charge densities in the diffuse layer (σ_{dif}) and on the oxide surface (σ_{ox}) can be calculated using the site-bonding model through (*34*, *35*)

$$\sigma_{dif} = \sqrt{8kT\varepsilon_w N_{Avo} c_{HCl}} \sinh\left(\frac{q(V_G - V_0 - \psi_{dif})}{kT}\right) \quad (4)$$

$$\sigma_{ox} = qN_{OH}\left(\frac{{c_{Hs}}^2 - K_a K_b}{K_a K_b + K_b c_{Hs} + {c_{Hs}}^2}\right) \quad (5)$$

where ε_w is the dielectric constant of water, N_{Avo} is the Avogadro's number, and K_a and K_b are the equilibrium constants of the surface reaction between Si—OH and H^+. Meanwhile, σ_{dif} is also related to the Stern layer capacitance C_{st} through

$$\sigma_{dif} = (\psi_{dif} - \psi_{Si})\, C_{st} \quad (6)$$

Last, charge neutrality requires

$$\sigma_{ox} + \sigma_{dif} + \sigma_{Si} = 0 \quad (7)$$

As the constant parameters V_0 and C_{st} are preset, potential and charge distribution can be solved by combining Eqs. 2 to 7. When V_0 = 60 mV and $C_{st} = 4 \times 10^{-5}$ F, the solved potential and charge distribution can fit the time constants in Figs. 3 and 4 quite well using Eq. 1. The extracted k_{on} and k_{off} are listed in table S1.

SUPPLEMENTARY MATERIALS

Supplementary material for this article is available at https://science.org/doi/10.1126/sciadv.abj6711

REFERENCES AND NOTES

1. W. Gao, S. Emaminejad, H. Y. Y. Nyein, S. Challa, K. Chen, A. Peck, H. M. Fahad, H. Ota, H. Shiraki, D. Kiriya, D.-H. Lien, G. A. Brooks, R. W. Davis, A. Javey, Fully integrated wearable sensor arrays for multiplexed in situ perspiration analysis. *Nature* **529**, 509–514 (2016).
2. Y. Cui, Q. Wei, H. Park, C. M. Lieber, Nanowire nanosensors for highly sensitive and selective detection of biological and chemical species. *Science* **293**, 1289–1292 (2001).
3. H.-M. So, K. Won, Y. H. Kim, B.-K. Kim, B. H. Ryu, P. S. Na, H. Kim, J.-O. Lee, Single-walled carbon nanotube biosensors using aptamers as molecular recognition elements. *J. Am. Chem. Soc.* **127**, 11906–11907 (2005).
4. A. Star, E. Tu, J. Niemann, J.-C. P. Gabriel, C. S. Joiner, C. Valcke, Label-free detection of DNA hybridization using carbon nanotube network field-effect transistors. *Proc. Natl. Acad. Sci. U.S.A.* **103**, 921–926 (2006).
5. J. Salfi, I. G. Savelyev, M. Blumin, S. V. Nair, H. E. Ruda, Direct observation of single-charge-detection capability of nanowire field-effect transistors. *Nat. Nanotechnol.* **5**, 737–741 (2010).
6. N. K. Rajan, D. A. Routenberg, M. A. Reed, Optimal signal-to-noise ratio for silicon nanowire biochemical sensors. *Appl. Phys. Lett.* **98**, 264107–2641073 (2011).
7. S. Sorgenfrei, C.-Y. Chiu, R. L. Gonzalez Jr., Y.-J. Yu, P. Kim, C. Nuckolls, K. L. Shepard, Label-free single-molecule detection of DNA-hybridization kinetics with a carbon nanotube field-effect transistor. *Nat. Nanotechnol.* **6**, 126–132 (2011).
8. S. Sorgenfrei, C.-Y. Chiu, M. Johnston, C. Nuckolls, K. L. Shepard, Debye screening in single-molecule carbon nanotube field-effect sensors. *Nano Lett.* **11**, 3739–3743 (2011).
9. J. Li, G. He, H. Ueno, C. Jia, H. Noji, C. Qi, X. Guo, Direct real-time detection of single proteins using silicon nanowire-based electrical circuits. *Nanoscale* **8**, 16172–16176 (2016).
10. N. Singh, K. D. Buddharaju, S. K. Manhas, A. Agarwal, S. C. Rustagi, G. Q. Lo, N. Balasubramanian, D.-L. Kwong, Si, SiGe nanowire devices by top–down technology and their applications. *IEEE Trans. Electron. Devices* **55**, 3107–3118 (2008).
11. I. Park, Z. Li, A. P. Pisano, R. S. Williams, Top-down fabricated silicon nanowire sensors for real-time chemical detection. *Nanotechnology* **21**, 015501 (2010).
12. S. Chen, J. G. Bomer, E. T. Carlen, A. van den Berg, Al_2O_3/silicon nanoISFET with near ideal Nernstian response. *Nano Lett.* **11**, 2334–2341 (2011).
13. M. Wipf, R. L. Stoop, A. Tarasov, K. Bedner, W. Fu, I. A. Wright, C. J. Martin, E. C. Constable, M. Calame, C. Schönenberger, Selective sodium sensing with gold-coated silicon nanowire field-effect transistors in a differential setup. *ACS Nano* **7**, 5978–5983 (2013).
14. O. Knopfmacher, A. Tarasov, W. Fu, M. Wipf, B. Niesen, M. Calame, C. Schönenberger, Nernst limit in dual-gated Si-nanowire FET sensors. *Nano Lett.* **10**, 2268–2274 (2010).
15. K. Martens, S. Santermans, M. Gupta, G. Hellings, R. Wuytens, B. D. Bois, E. Dupuy, E. Altamirano-Sanchez, K. Jans, R. Vos, T. Stakenborg, L. Lagae, M. Heyns, S. Severi, W. V. Roy, BioFET technology: Aggressively scaled pMOS FinFET as biosensor, in *Proceedings of the 2019 IEEE International Electron Devices Meeting (IEDM)*, San Francisco, CA, USA, 7 to 11 December 2019.
16. E. Stern, J. F. Klemic, D. A. Routenberg, P. N. Wyrembak, D. B. Turner-Evans, A. D. Hamilton, D. A. LaVan, T. M. Fahmy, M. A. Reed, Label-free immunodetection with CMOS-compatible semiconducting nanowires. *Nature* **445**, 519–522 (2007).
17. N. Clément, K. Nishiguchi, J. F. Dufreche, D. Guerin, A. Fujiwara, D. Vuillaume, A silicon nanowire ion-sensitive field-effect transistor with elementary charge sensitivity. *Appl. Phys. Lett.* **98**, 014104 (2011).
18. E. Simoen, C. Claeys, On the flicker noise in submicron silicon MOSFETs. *Solid State Electron.* **43**, 865–882 (1999).
19. C. G. Theodorou, E. G. Ioannidis, F. Andrieu, T. Poiroux, O. Faynot, C. A. Dimitriadis, G. Ghibaudo, Low-frequency noise sources in advanced UTBB FD-SOI MOSFETs. *IEEE Trans. Electron. Devices* **61**, 1161–1167 (2014).
20. M. J. Deen, M. W. Shinwari, J. C. Ranuárez, Noise considerations in field-effect biosensors. *J. Appl. Phys.* **100**, 074703 (2006).
21. S. Bangsaruntip, G. M. Cohen, A. Majumdar, Y. Zhang, S. U. Engelmann, N. C. M. Fuller, L. M. Gignac, S. Mittal, J. S. Newbury, M. Guillorn, T. Barwicz, L. Sekaric, M. M. Frank, J. W. Sleight, High performance and highly uniform gate-all-around silicon nanowire MOSFETs with wire size dependent scaling, in *Proceedings of the 2019 IEEE International Electron Devices Meeting (IEDM)*, Baltimore, MD, USA, 7 to 9 December 2009.
22. S.-W. Ryu, K. Min, J. Shin, H. Kwon, D. Nam, T. Oh, T.-S. Jang, M. Yoo, Y. Kim, S. Hong, Overcoming the reliability limitation in the ultimately scaled DRAM using silicon migration technique by hydrogen annealing, in *Proceedings of the 2017 IEEE International Electron Devices Meeting (IEDM)*, San Francisco, CA, USA, 2 to 6 December 2017.
23. S. Zafar, C. D'Emic, A. Jagtiani, E. Kratschmer, X. Miao, Y. Zhu, R. Mo, N. Sosa, H. Hamann, G. Shahidi, H. Riel, Silicon nanowire field effect transistor sensors with minimal sensor-to-sensor variations and enhanced sensing characteristics. *ACS Nano* **12**, 6577–6587 (2018).
24. A. H. Edwards, Interaction of H and H_2 with the silicon dangling orbital at the ⟨111⟩ Si/SiO_2 interface. *Phys. Rev. B Condens. Matter* **44**, 1832–1838 (1991).
25. G. W. Trucks, K. Raghavachari, G. S. Higashi, Y. J. Chabal, Mechanism of HF etching of silicon surfaces: A theoretical understanding of hydrogen passivation. *Phys. Rev. Lett.* **65**, 504–507 (1990).
26. E. Yablonovitch, D. L. Allara, C. C. Chang, T. Gmitter, T. B. Bright, Unusually low surface-recombination velocity on silicon and germanium surfaces. *Phys. Rev. Lett.* **57**, 249–252 (1986).
27. Z. Shi, J.-P. Mieville, M. Dutoit, Random telegraph signals in deep submicron n-MOSFET's. *IEEE Trans. Electron. Devices* **41**, 1161–1168 (1994).
28. J. Li, S. Pud, M. Petrychuk, A. Offenhäusser, S. Vitusevich, Sensitivity enhancement of Si nanowire field effect transistor biosensors using single trap phenomena. *Nano Lett.* **14**, 3504–3509 (2014).
29. P. M. Lenahan, T. D. Mishima, J. Jumper, T. N. Fogarty, R. T. Wilkins, Direct experimental evidence for atomic scale structural changes involved in the interface-trap transformation process. *IEEE Trans. Nucl. Sci.* **48**, 2131–2135 (2001).
30. O. Stern, Zur theorie der elektrolytischen doppelschicht. *Z. Elektrochem. Angew. Phys. Chem.* **30**, 508–516 (1924).
31. R. E. G. van Hal, J. C. T. Eijkel, P. Bergveld, A novel description of ISFET sensitivity with the buffer capacity and double-layer capacitance as key parameters. *Sens. Actuators B* **24**, 201–205 (1995).
32. D. Landheer, G. Aers, W. R. McKinnon, M. J. Deen, J. C. Ranuarez, Model for the field effect from layers of biological macromolecules on the gates of metal-oxide-semiconductor transistors. *J. Appl. Phys.* **98**, 044701 (2005).
33. M. J. Kirton, M. J. Uren, Noise in solid-state microstructures: A new perspective on individual defects, interface states and low-frequency (1/*f*) noise. *Adv. Phys.* **38**, 367–468 (1989).
34. R. E. G. van Hal, J. C. T. Eijkel, P. Bergveld, A general model to describe the electrostatic potential at electrolyte oxide interfaces. *Adv. Colloid Interface Sci.* **69**, 31–62 (1996).

35. D. Landheer, W. R. McKinnon, G. Aers, W. Jiang, M. J. Deen, M. W. Shinwari, Calculation of the response of field-effect transistors to charged biological molecules. *IEEE Sens. J.* **7**, 1233–1242 (2007).
36. S. T. Martin, G. P. Li, E. Worley, J. White, The gate bias and geometry dependence of random telegraph signal amplitudes [MOSFET]. *IEEE Electron. Device Lett.* **18**, 444–446 (1997).
37. K. K. Hung, P. K. Ko, C. Hu, Y. C. Cheng, A unified model for the flicker noise in metal-oxide-semiconductor field-effect transistors. *IEEE Trans. Electron. Devices* **37**, 654–665 (1990).
38. R. Jayaraman, C. G. Sodini, A 1/*f* noise technique to extract the oxide trap density near the conduction band edge of silicon. *IEEE Trans. Electron. Devices* **36**, 1773–1782 (1989).
39. Y. Liu, L. Shen, From Langmuir kinetics to first- and second-order rate equations for adsorption. *Langmuir* **24**, 11625–11630 (2008).
40. T. M. Squires, R. J. Messinger, S. R. Manalis, Making it stick: Convection reaction and diffusion in surface-based biosensors. *Nat. Biotechnol.* **26**, 417–426 (2008).

Acknowledgments
Funding: This work was supported by Swedish Strategic Research Foundation FFL15-0174 (Z.Z.), Swedish Research Council 2014-5588 and 2019-04690 (Z.Z.), and Wallenberg Academy Fellow program 2015-0127 (Z.Z.). **Author contributions:** Z.Z. conceived the idea and initiated the project. Q.H. and Z.Z. designed the experiments. Q.H. performed device fabrication, liquid measurements, data analysis, and modeling under the supervision of S.C., P.S., and Z.Z. Q.H. wrote the manuscript. S.C., P.S., and Z.Z. analyzed the data and revised the manuscript. **Competing interests:** The authors declare that they have no competing interests. **Data and materials availability:** All data needed to evaluate the conclusions in the paper are present in the paper and/or the Supplementary Materials.

Submitted 30 May 2021
Accepted 14 October 2021
Published 3 December 2021
10.1126/sciadv.abj6711

ScienceAdvances

Ion sensing with single charge resolution using sub–10-nm electrical double layer–gated silicon nanowire transistors

Qitao HuSi ChenPaul SolomonZhen Zhang

Sci. Adv., 7 (49), eabj6711. • DOI: 10.1126/sciadv.abj6711

Science Advances (ISSN) is published by the American Association for the Advancement of Science. 1200 New York Avenue NW, Washington, DC 20005. The title *Science Advances* is a registered trademark of AAAS.